Journal of
Data Acquisition and Processing
ISSN: 1004-9037
https://sjcjycl.cn/
DOI: 10.5281/zenodo.7765932

DOUBLE CATTANEO-CHRISTOV DIFFUSION EFFECTS OF MAXWELL-NANOFLUID RADIATIVE FLOW PAST A STRETCHED SHEET IN PRESENCE OF DOUBLE DIFFUSION EFFECTS

Khaja Hassan [1], R. Vijaya Kumar [2] and G. Srinivas [3]

[1]Department of Mathematics, Guru Nanak Institute of Technology, Khanapur, Ibrahimpatnam, Hyderabad, 501506, Telangana State, India.

[2]Mathematics Section, Faculty of Engineering and Technology, Annamalai University, Annamalainagar, Chidambaram-608002, Tamilnadu, India.

Department of Mathematics, Periyar Government Arts College, Cuddalore, 607001, Tamilnadu State, India.

[3]Department of Mathematics, Guru Nanak Institute of Technology, Khanapur, Ibrahimpatnam, Hyderabad, 501506, Telangana State, India.

[2]Corresponding author Email address: rathirath_viji@yahoo.co.in

Abstract:. The Cattaneo-Christov dual diffusion method is used to study heat and mass dispersion. Similarity variables are accustomed to reduce fluid flow partial differential equations to linear ordinary differential equations in this research. This study solves the system of ordinary differential equations using the finite element method. This analysis shows the impact of physical factors such fluid velocity, temperature, concentration, skin friction, heat and mass transfer rates. This investigation shows the skin-friction coefficient and Nusselt number for several flow-related factors in tabular and graphical modes. These graphs allow inferences and verify results.

Keywords: Double Cattaneo-Christov diffusion; Maxwell fluid; Nanofluid; Thermal radiation; stretching sheet; Cross diffusion; Finite element method.

Nomenclature:

List of Symbols:

u, v :	Velocity components in x and y axes respectively (m/s)
x, y :	Measuring along the stretching sheet in Cartesian coordinates(m)
f :	Dimensionless stream function
f' :	Fluid velocity (m/s)
$\Pr$:	Prandtl number
Du :	Modified Dufour parameter
Sr :	Dufour solutal Lewis number
C :	Concentration of Fluid$\left(mol/m^3\right)$
B_o :	Uniform magnetic field
C_∞ :	Dimensional ambient volume fraction $\left(mol/m^3\right)$
T :	Fluid temperature (K)
T_f :	Convective surface temperature(K)
T_∞ :	Temperature of the fluid far away from the stretching sheet (K)
O :	Origin
M :	Magnetic field parameter
Cf :	coefficient of Skin-friction

Introduction:

C_w: stretching surface for Dimensional concentration $\left(mol/m^3\right)$

Nu: Rate of heat transfer coefficient (or) Nusselt number

Sh: Rate of mass transfer coefficient (or) Sherwood number

C_p: Specific heat capacity of nanoparticle material

Sc: Schmidt number

Nb: Brownian Motion parameter

Nt: Thermophoresis parameter

D_B: Brownian diffusion coefficient

D_T: Thermophoresis diffusion coefficient

D_{CT}: Soret diffusivity

R: Thermal radiation parameter

h_f: Convective heat transfer coefficient

D_{TC}: Dufour diffusivity

fw: Suction/Injection parameter

Bi: Biot number

K: Permeability parameter

k_1: Dimensional permeability parameter

Q_o: Dimensional heat absorption/ generation parameter

$Q>0$: Heat absorption parameter

$Q<0$: Heat generation parameter

a: Positive real number

Re_x: Reynold's number

u_w: Velocity of the sheet

$v_w>0$: Suction

$v_w<0$: Injection

Greek symbols:

η: Dimensionless similarity variable

θ: Dimensionless temperature (K)

ϕ: Dimensionless nanofluid concentration $\left(mol/m^3\right)$

ν: Kinematic viscosity $\left(m^2/s\right)$

σ: Electrical conductivity

ρ: Density of the fluid

σ^*: Stefan-Boltzmann constant

λ: Maxwell fluid parameter (or) Deborah number

ψ: Stream function

γ: Thermal relaxation time parameter

ζ: Mass relaxation time parameter

κ: Thermal conductivity of the fluid

β: Relaxation time of the fluid

λ_T: Thermal relaxation time

λ_C: Mass relaxation time

Superscript:

$'$: Differentiation w.r.t η

Subscripts:

f: Fluid

w: Condition on the sheet

∞: Ambient Conditions

1. Introduction:

The constitutive equations of a material serve as a guide for categorising its rheological characteristics. The Navier-Stokes equation is the fundamental description of this fluid, and the Newtonian constitutive equation is easy to solve. Because of the crucial role they play in the disciplines of engineering and industry, non-Newtonian fluids have recently attracted the interest of academics and scientists. Suspension solutions, Liquid crystals, polymer fluids, colloidal solutions, , unusual lubricants and the circulation of animal blood are some examples. Since they are complexity, no constitutive equation can fully describe non-Newtonian fluids. This property motivated the development of numerous non-Newtonian fluid models in earlier investigations. A fascinating kind of viscoelastic fluid that may be utilised to show the uniqueness of fluid relaxation time is the upper convicted Maxwell fluid. This allows us to concentrate on the effect of liquid elasticity taking place boundary layer properties rather than the more complicated impacts of shear-dependent viscosity. The Maxwell fluid, which stands recognised as a frequency form, includes lubricants, polymer solutions, and crude oil as examples. Harris [1] developed the basic equations for the upper-convicted Maxwell's boundary layer flow in two dimensions. For the first time, Maxwell [2] used his fluid model to explain the elasticity and viscosity of air. Zhang et al. [3] investigated how Newtonian heating and sliding impact Maxwell fluids in natural convection. Sadeghy and colleagues [4] investigated Sakiadis' Maxwell fluid movement. Hayat et al. [5] provided mathematical modelling for two-dimensional MHD Maxwell fluid flow induced by a moving surface. Jian and Li investigated microtube Maxwell fluid flow [6]. Raftari and Yildirim [7] addressed magnetohydrodynamic Maxwell fluid flow across a porous surface via homotopy perturbation. Singh and Agarwal [8] investigated heat transmission and Maxwell fluid MHD flow in a porous material with varying thermal conduction. Naveed et al. [9] investigated Maxwell nanofluid flow stability over a decreasing superficial. Khan and Nadeem [10] used the Maxwell nanofluid model on a decreasing sheet to find the various approaches to the MHD impact at stagnation. Billal, Singh, and Sheikholeslmi used the Shooting scheme and the fourth-order Runge Kutta (RK) technique to analyse Maxwell fluid with a focus on MHD and nonlinear thermal radiation. Fourier's law, employed in classical physics [14], underpins heat transfer processes.The determinism assumption and how certain perturbations influence the whole medium are the main problems with the parabolic heat equation. In technological and environmental systems, fluid flow is commonplace in places like reservoirs, geothermal energy systems, catalytic reactors, and the dumping of crude oil. The Cattaneo thermal tranquillity provides the framework for the Fourier law of thermal conduction [15]. A hyperbolic energy function is mentioned in Cattaneo. In order to attain product separability, the Christov model [16] expanded the Cattaneo rule by including temporal relaxation into Oldroyd's canteen model. Another heat flow model shows the Cattaneo-Christov model. Radiation, Joule heating, Cattaneo-Christov fields, and magnetic fields alter Blasius-Rayleigh-Stokes fluid flow, according to Reddy et al. [17]. Haneef et al. used an Oldroyd-B nano-liquid hybrid for Cattaneo-Christov heat transfer [18]. Gowda et al. examined the Cattaneo-Christov concept in flow of nanofluid on curved lines. [19]. Mubaddel et al. [20] employed heat radiation and Cattaneo-Christov flux to explore Nanoscale nano-liquid bio-convection flow. Ijaz and Ayub [21] described nonlinear convective Maxwell stratified nanofluid flow using the CattaneoChristov heat flux model and an inclined stretched cylinder with activation energy. Shehzad et al. [22] observed that the Cattaneo-Christov theory of mass and heat diffusions retarded mass and thermal profiles in this chemically sensitive MHD Maxwell fluid movement model. Hayat et al [23] examined how the Cattaneo-Christovmodel of heat flux impacts stagnation point outflow heat transfer. Mustafa [24] examined Maxwell fluid rotation with surface motion using the Cattaneo-Christovmodel of heat flux. Logical inferences Abbasi et al. [25] examined the Oldroyd-B fluid boundary layer flow Cattaneo-Christovmodel of heat flux. Waqas et al. [26] investigated the Cattaneo-Christov heat flow typical for aambiguous Burgers liquid with changing thermal conduction. Shehzad et al. [27] used the Cattaneo-Christovmodel of heat flux to study fluid movement in an exponential growth of stretched sheet. Han et al. [28] employed Cattaneo-verbalization to describe heat transfer in a Maxwell liquid with a stretched plate. Ali et al. [29] of Christovpractised the Cattaneo-Christovmodel of heat flux to study thermal convection and radiation on unsteady MHD Blasius and Sakiadis flow. The CattaneoChristovmodel of heat flux is used to quantitatively examine two-dimensional, viscous, electrical conduction, incompressible, continuous Maxwell-nanofluid flow across a stretched porous sheet. The similarity transformation converts the flow model PDEs obsessed by ODEs, which are addressed bythe finite element method, a common numerical approach. The sheet surface heat,skin-friction, and mass transfer charges characterise momentum, thermal, and species flow field boundary layer profiles. Paper, plastic films, cooling metal sheets, and crystals are made using this numerical analysis.

Flow Governing Equations:

We perform an investigation into a continuous two-dimensional flow of viscous incompressible electrical conduction MHD Maxwell-Nanofluid across a stretched sheet in porous media. There is consideration given to both cross and double Cattaneo-Christov diffusion. The following are presumptions made throughout this investigation:

- This incompressible, viscous, electrically conducting fluid flow is two-dimensional.
- A uniform Bo is appealed in the u-direction, the impelled magnetic field be situatedto be neglected because Ohmic dissipation and small magnetic Reynolds number, and and Hall current impacts are unnoticed as the magnetic field stands weak.
- We also assume that the surface concentration and temperature are the ambient temperature and concentration.

Fig. 1 shows the physical and schematic arrangement through the elaborated model coordinate system.

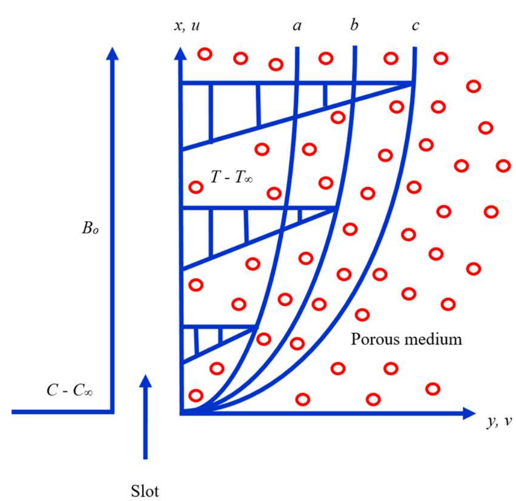

a ------Momentum boundarylayer, b ------ Thermal boundarylayer, c ------ Concentration boundarylayer

Fig. 1. Physical geometry of the flow field

The Maxwell-Nanofluid is a type of fluid that contains suspended nano particles. To describe the behaviour of such a fluid, we can use the following set of equations:

Continuity Equation:

$$\frac{\partial u}{\partial x}+\frac{\partial u}{\partial y}=0 \tag{1}$$

Momentum Equation:

$$u\left(\frac{\partial u}{\partial x}\right)+v\left(\frac{\partial u}{\partial y}\right)=\nu\left(\frac{\partial^2 u}{\partial y^2}\right)-\left(\frac{\sigma B_o^2}{\rho}\right)u-\nu\left(\frac{u}{k_1}\right)-\beta\left(u^2\frac{\partial^2 u}{\partial x^2}+v^2\frac{\partial^2 u}{\partial y^2}+2uv\frac{\partial^2 u}{\partial x\partial y}\right) \tag{2}$$

Equation of thermal energy:

$$u\left(\frac{\partial T}{\partial x}\right)+v\left(\frac{\partial T}{\partial y}\right)=\frac{\kappa}{\rho C_p}\left(1+\frac{16\sigma^* T_\infty^3}{3\rho C_p\kappa_T}\right)\left(\frac{\partial^2 T}{\partial y^2}\right)+\tau\left\{D_B\left(\frac{\partial C}{\partial y}\right)\left(\frac{\partial T}{\partial y}\right)+\frac{D_T}{T_\infty}\left(\frac{\partial T}{\partial y}\right)^2\right\}+D_{TC}\left(\frac{\partial^2 C}{\partial y^2}\right)$$

$$-\lambda_T\left(u^2\frac{\partial^2 T}{\partial x^2}+v^2\frac{\partial^2 T}{\partial y^2}+\left(u\frac{\partial u}{\partial x}+v\frac{\partial u}{\partial y}\right)\frac{\partial T}{\partial x}+2uv\frac{\partial^2 T}{\partial x\partial y}\right)+\left(u\frac{\partial u}{\partial x}+v\frac{\partial u}{\partial y}\right)\frac{\partial T}{\partial y}+\frac{Q_o}{\rho C_p}\left(T-T_\infty\right)$$

(3)

Equation of species concentration:

$$u\left(\frac{\partial C}{\partial x}\right)+v\left(\frac{\partial C}{\partial y}\right)=D_B\left(\frac{\partial^2 C}{\partial y^2}\right)+\frac{D_T}{T_\infty}\left(\frac{\partial^2 T}{\partial y^2}\right)+D_{CT}\left(\frac{\partial^2 T}{\partial y^2}\right)-$$

$$\lambda_C\left(u^2\frac{\partial^2 C}{\partial x^2}+v^2\frac{\partial^2 C}{\partial y^2}+\left(u\frac{\partial u}{\partial x}+v\frac{\partial u}{\partial y}\right)\frac{\partial C}{\partial x}+2uv\frac{\partial^2 C}{\partial x\partial y}\right)+\left(u\frac{\partial u}{\partial x}+v\frac{\partial u}{\partial y}\right)\frac{\partial C}{\partial y} \tag{4}$$

For Double Cattaneo-Christov diffusion effects of Maxwell-Nanofluid, the corresponding boundary conditions are

$$\left.\begin{array}{l} u=u_w,\ v=-v_w,\ -\kappa\dfrac{\partial T}{\partial y}=h_f\left(T_f-T_\infty\right),\ C=C_w\ \ at\ \ y=0 \\ u\to 0,\ T\to T_\infty,\ C\to C_\infty\ \ as\ \ y\to\infty \end{array}\right\} \tag{5}$$

In order to solve governing equations, the subsequent similarity variables are presented below. (2)-(4)as

$$\left.\begin{array}{l} \eta=y\sqrt{\frac{a}{\nu}},\psi=\left(\sqrt{a\nu}\right)xf(\eta),u=\frac{\partial\psi}{\partial y},v=-\frac{\partial\psi}{\partial x}, \\ u=axf'(\eta),v=-\left(\sqrt{a\nu}\right)f(\eta),\theta=\frac{T-T_\infty}{T_f-T_\infty},\phi=\frac{C-C_\infty}{C_w-C_\infty} \end{array}\right\} \tag{6}$$

Using Eq. (6), the fundamental Eqs. (2) to (4) become

$$f'''+ff''-f'^2-Mf'-Kf'-\lambda\left(f^2f''-2ff'f''\right)=0 \tag{7}$$

$$\left(1+\frac{4R}{3}\right)\theta''+\Pr f\theta'+\Pr Nb\theta'\phi'+\Pr Nt\theta'^2-\Pr\gamma\left(f^2\theta''+ff'\theta'\right)+\Pr Q\theta+\Pr Du\phi''=0 \tag{8}$$

$$Nb\phi''+NbScf\phi'+NtSc\theta''+ScSrNb\theta''-Sc\zeta\left(f^2\phi''+ff'\phi'\right)=0 \tag{9}$$

and the corresponding boundary conditions (5) become

$$\left.\begin{array}{l} f(0)=fw,\ f'(0)=1,\ \theta'(0)=-Bi\left[1-\theta(0)\right],\ \phi(0)=1\ \ at\ \ \eta=0 \\ f'\to 0,\ \theta\to 0,\ \phi\to 0\ \ as\ \ \eta\to\infty \end{array}\right\} \tag{10}$$

where the elaborated physical parameters are defined as

$$\left.\begin{array}{l}\lambda=\beta a,\ \Pr=\dfrac{\nu\rho C_p}{\kappa},\ R=\dfrac{4\sigma^{*}T_\infty^{3}}{\kappa\kappa_T},\ M=\dfrac{\sigma B_o^2}{\rho a},\ Q=\dfrac{Q_o}{a\rho C_p},\ Sc=\dfrac{\nu}{D_B},\\ Nb=\dfrac{(\rho C)_f D_B(C_w-C_\infty)}{(\rho C)_p\nu},\ Nt=\dfrac{(\rho C)_f D_T(T_f-T_\infty)}{(\rho C)_p T_\infty},\ Du=\dfrac{D_{TC}(C_w-C_\infty)}{\alpha(T_f-T_\infty)},\\ Sr=\dfrac{D_{CT}(T_f-T_\infty)}{D_B(C_w-C_\infty)},\ \gamma=a\lambda_T,\ \zeta=a\lambda_C,\ Bi=\dfrac{h_f}{\kappa}\sqrt{\dfrac{\nu}{a}},\ K=\dfrac{\nu}{ak_1},\end{array}\right\} \quad (11)$$

In heat and mass transfer issues, engineers are interested in the Sherwood number, local Nusselt number, and Skin-friction coefficient. These factors determine things like mass transfer rates, wall heat transfer rates, and skin-friction coefficients.

$$\sqrt{\mathrm{Re}_x}Cf=2(1+\lambda)f''(0) \quad (12)$$

$$\frac{Nu}{\sqrt{\mathrm{Re}_x}}=-\left(1+\frac{4R}{3}\right)\theta'(0) \quad (13)$$

$$\frac{Sh}{\sqrt{\mathrm{Re}_x}}=-\phi'(0) \quad (14)$$

Numerical Solutions by Finite Element Method:

Here partial and ordinary differential equations will be solved by using finite element method. This solves differential equations well. As said, the finite element approach divides the domain into finite-dimensional elements. This was the most flexible numerical engineering analysis method when released. Its use has helped fluid mechanics, heat transport, solid mechanics, rigid body dynamics, electrical systems, chemical processes, and acoustics. Fig. 2 shows the finite element method. These steps must precede a finite element analysis.

Domain discretization into elements: With the use of finite elements, the entire interval is broken up obsessed by a certain number of smaller intervals, who are referred to as elements.

Domain decomposition into elements: The finite-element mesh is made up of all of the elements that were previously mentioned.

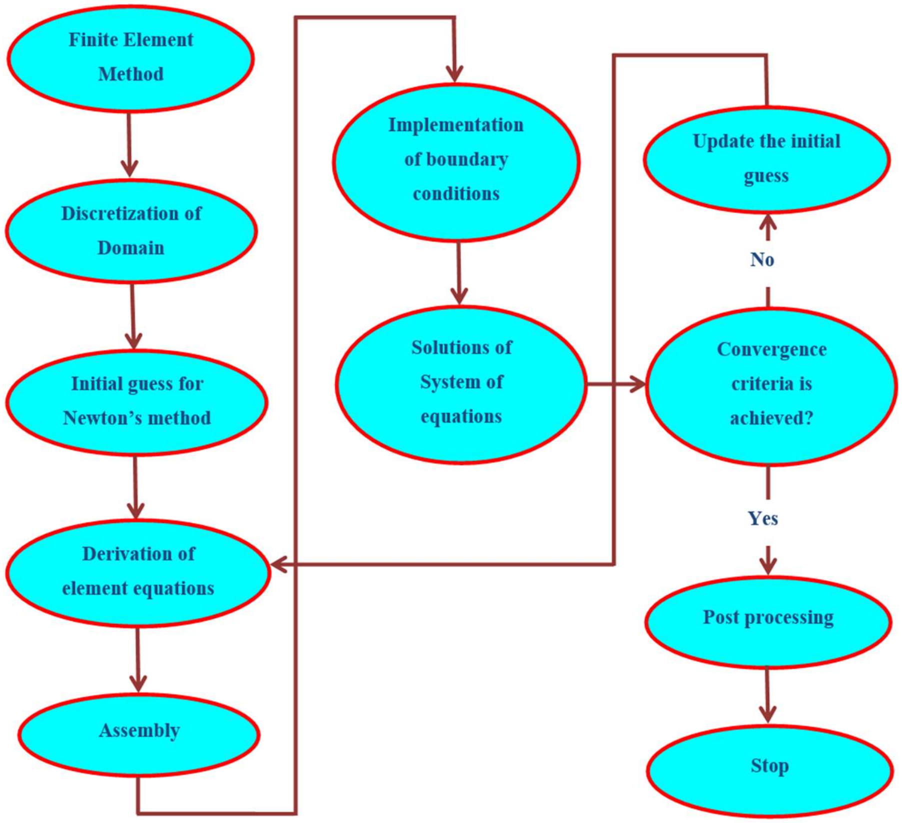

Fig. 2. Finite Element Method flow chart

To generate element equations, the following technique should be followed:

a) Initial variations of the mathematical model are made over the typical element (a single element from the mesh).
b) When the variational problem has an approximate solution, the fundamental equations constructed by replacing the estimated solution into the previously established structure, in which solved for the variable.
c) This matrix is formed by interpolating polynomials and is referred to as stiffness matrix.

- Putting together and solving equations: All algebraic equations must be constructed by placing restrictions on each equation's constituents regarding inter-element continuity. By tying a lot of algebraic equations together, A global finite-element model of the entire domain is realisable.
- Establishing boundary conditions: It is important to apply the boundary conditions of the flow model to the created equations.

Built equations may be solved using a variety of numerical approaches, including the LU decomposition method, the Gauss elimination method, and others. When working with real numbers, it is essential to remember the form functions used to approximate real functions. There are a total of 20,001 nodes in the flow domain, which is partitioned into 10,000 similarly sized quadratic components. The flow domain is made up of 10,000 similar-sized quadratic components. After creating the element equations, we were provided with 80,004 nonlinear equations for analysis. After applying the boundary conditions, the remaining system of nonlinear equations is solved numerically using the Gauss elimination technique with a precision of 0.00001. The use of Gaussian quadrature facilitates the solution of integrations. The computer application for the approach was created using the MATHEMATICA programming language and ran on a desktop computer.

Program Code Validation:

Table-1.: Code validation results with present Skin-friction coefficient results obtained by Mukhopadhyay [30] and Sadghey et al. [31] for different values of λ by fixing $M = K = Sr = Du = 0$.

λ	Mukhopadhyay [30] results	Sadghey et al. [31] results	Present numerical results
0.0	0.9999963	1.000	1.00768398683683914763
0.2	1.051949	1.0549	1.1067866657401374686
0.4	1.101851	1.10084	1.10005380396934893398
0.6	1.150162	1.0015016	100067679637937387337
0.8	1.196693	1.19872	101867686639763939731

For scrutiny of code validation, the present numerical Skin-friction results are compared to Mukhopadhyay's published results. [30] and Sadghey et al. [31] in table-1for . From this table,The finite element approach, which has converged up to twenty decimal places, and the current results are in good accord, it is observed.

Results and Discussion:

Differentiated Flow Patterns Figures 3, 4, 5, 6, 7, 8, 9, 10, and 11 show the effects of varying the magnetic field (M), permeability (K), Deborah number (λ), suction/injection (fw), Prandtl number (Pr), thermal radiation (R), thermal relaxation time (γ), heat generation/absorption (Q), Soret number (Sr), Dufour number (Du), thermophoresis (Nt), Brownian motion (Nb), and Biot number (Bi), Schmidt Unless otherwise specified, the following values of the parameters are held constant throughout the computations: M = 0.5, K = 0.3, = 0.5, fw = 0.5, Pr = 0.71, R = 0.5, = 0.3, Q = 0.5, Sr = 0.5, Du = 0.5, Nt = 0.3, Nb = 0.5, Bi = 5.0, Sc = 0.22, ζ = 0.1. In Fig. 3 we see how varying the Permeability parameter (K) modifies the velocities. It was discovered that the accumulated permeability factor reduces the momentum and velocity limit layer. These results are more realistic because of the role friction plays in slowing down liquid motion. The effect of the ac field parameter M arranged velocity profiles is addressed with reference to Fig. 4. It was shown that the stream's velocity is inversely proportional to the magnetic parameter. For this reason, we can thank the Lorentz force, which is generated by an increase in the magnetic parameter. There is a generation of resistive force whenever a force is created that acts against the motion of fluid particles. Thisphenomena slows down the stream. The effect of the Deborah number (λ) on fluid velocity is shown in Fig. 5. Increasing improves the fluid's velocity. Yet, for Newtonian fluids, has the opposite effect, increasing the thickness of the boundary layer as increases. The relationship between Prandtl number (Pr) and fluid temperature is depicted in Fig. 7. When the Prandtl number (Pr) rises, the fluid's temperature gradient falls. Once the Prandtl number (Pr) is sufficiently high, momentum diffusivity overtakes thermal diffusivity. Faster heat dissipation and a thinner boundary layer are the results of the high fluid velocity, which improves heat transfer. In Fig. 8, we see how changing the thermal radiation parameter (R) affects the Maxwell-temperature Nanofluid's distribution. Increases in the nanofluid's temperature profile are clearly shown to be the result of a rise through radiation parameter (R) (see Fig. 8). Temperature distributions as a function of the thermal relaxation time parameter (γ) are displayed in Fig. 9. We can see from this graph that as the thermal relaxation time parameter is increased, the temperature profiles are reduced (γ). Figure 10 illustrates how the heat generation/absorption parameter (Q) influences the temperature distribution. Results display that a rise through heat generation parameter primes to an enlarge in the thermal boundary layer temperature and thickness, while the opposite is true in the case of heat absorption. Increased heat production is a natural by product of raising the heat generation parameter, and this in turn causes a hotter overall environment.

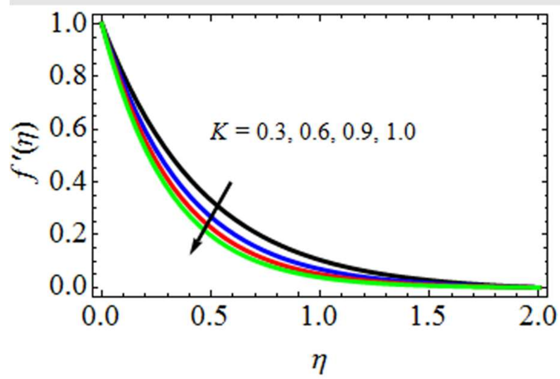

Fig. 3. K effect over the profiles of $f'(\eta)$

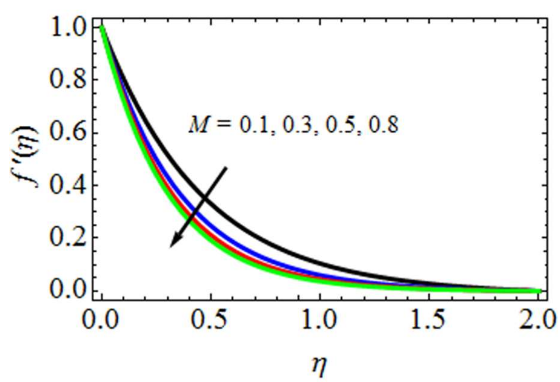

Fig. 4. M effect over the profiles of $f'(\eta)$

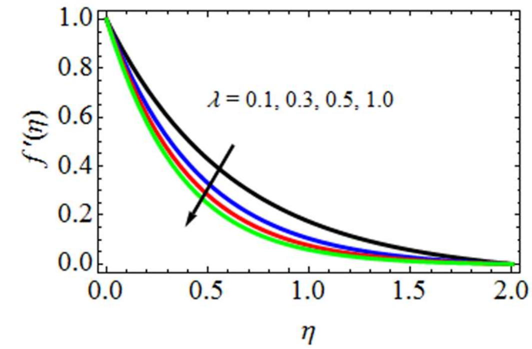

Fig. 5. λ effect over the profiles of $f'(\eta)$

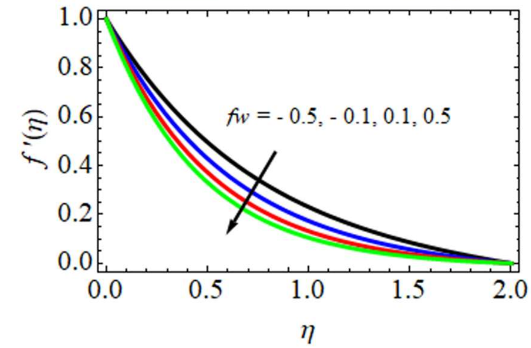

Fig. 6. Fw effect over the profiles of $f'(\eta)$

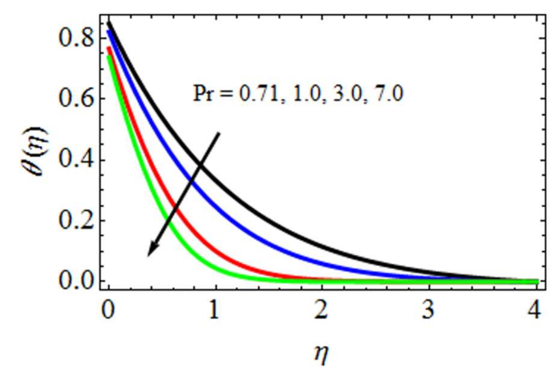

Fig. 7. Pr effect over the profiles of $\theta(\eta)$

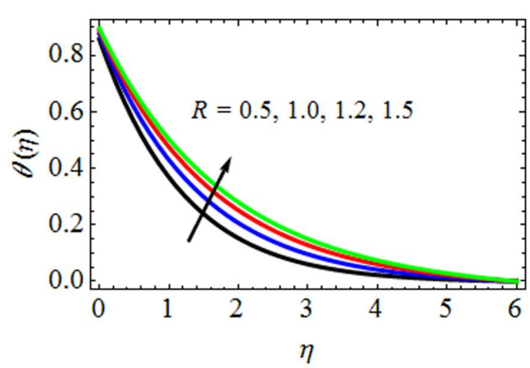

Fig. 8. R effect over the profiles of $\theta(\eta)$

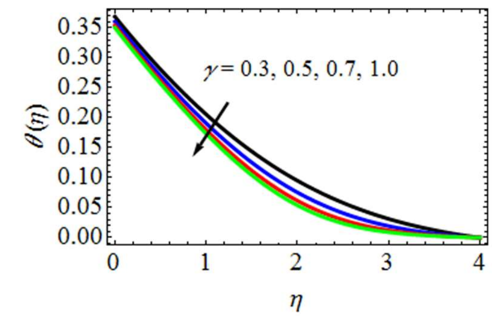

Fig. 9. γ effect over the profiles of $\theta(\eta)$

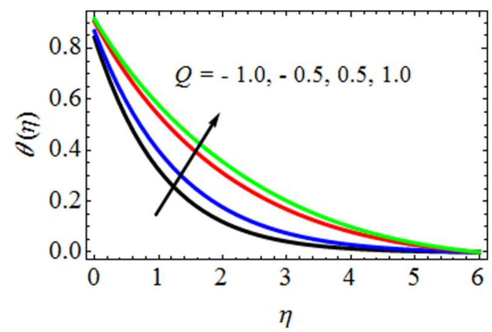

Fig. 10. Q influence on profiles of $\theta(\eta)$

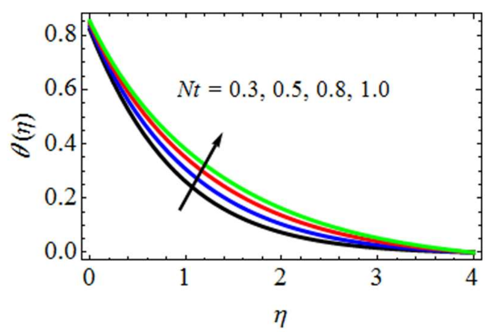

Fig. 11. Nt effect over the profiles of $\theta(\eta)$

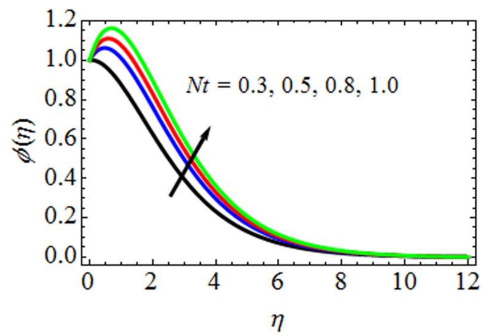

Fig. 12. Nt effect over the profiles of $\phi(\eta)$

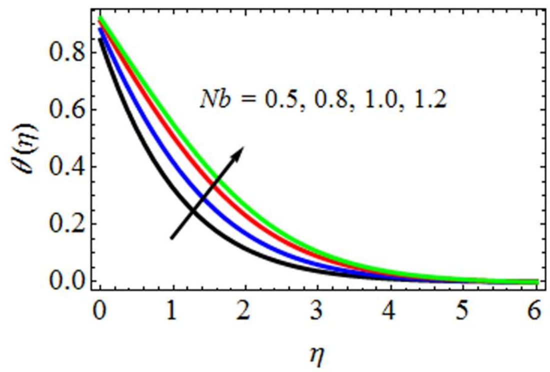

Fig. 13. *Nb* influence on profiles of $\theta(\eta)$

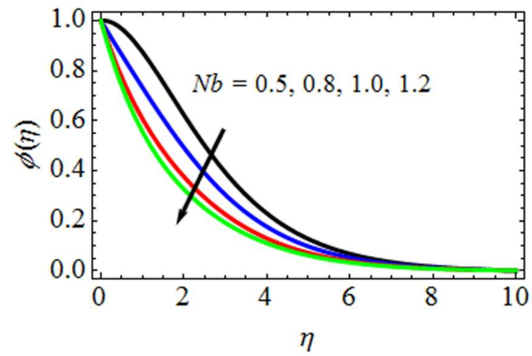

Fig. 14. *Nb* effect over the profiles of $\phi(\eta)$

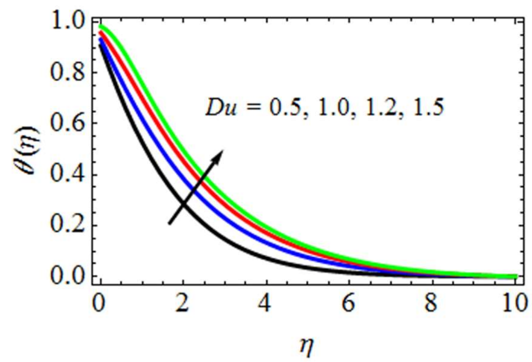

Fig. 15. *Du* effect over the profiles of $\theta(\eta)$

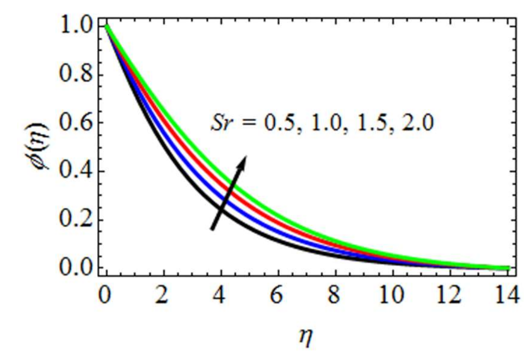

Fig. 16. *Sr* effect over the profiles of $\phi(\eta)$

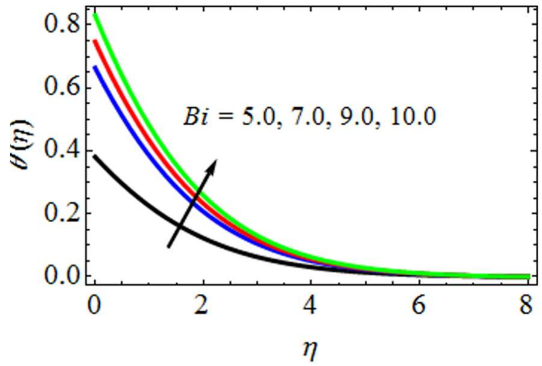

Fig. 17. Bi effect over the profiles of $\theta(\eta)$

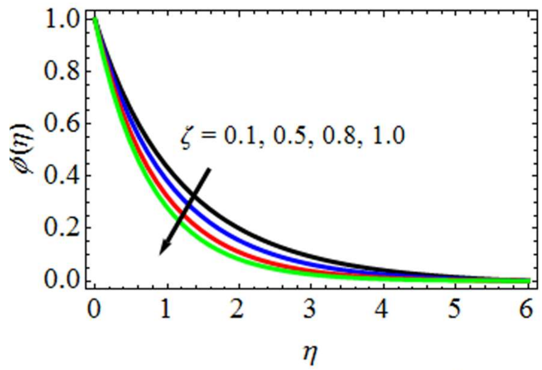

Fig. 18. ζ effect over the profiles of $\phi(\eta)$

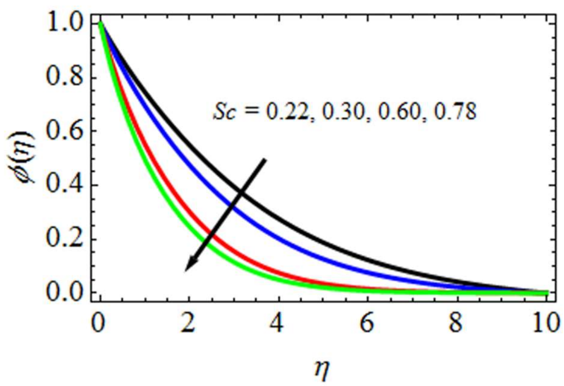

Fig. 19. Sc effect over the profiles of $\phi(\eta)$

Fig. 11 shows how the thermophoresis parameter (Nt) affects the distribution of the temperature. Figure 12 displays how Brownian motion parameter Nb disturbs concentration field. Raising Nb reduces the concentration field. The Brownian motion parameter (Nb) increases temperature and boundary layer thickness (see Fig. 13). Figure 14 demonstrates that concentration profile and boundary layer thickness increase with thermophoresis parameter. With higher thermophoresis parameters, nanoparticles enhance fluid heat conductivity. Figure 15 shows fluid temperature rising with Dufour number (Du). The system's temperature will rise if two chemically non-reacting fluids of the same temperature diffuse. Figure 16 shows that when Sr increases, fluid concentration rises. Non-reversible concentration field temperature gradients generate the Soret effect. This frequently increases flow system concentration flux. See Fig. 16.

Table-2.: Variation of *M*, *K*, *λ*, *fw*, Pr, *R*, *γ*, *Q*, *Sr*, *Du*, *Nt*, *Nb*, *Bi*, *Sc* and *ζ are given by values for the skin-friction coefficient*(*Cf*)

M	*K*	*λ*	*fw*	Pr	*R*	*γ*	*Q*	*Sr*	*Du*	*Nt*	*Nb*	*Bi*	*Sc*	*ζ*	*Cf*
0.5	0.3	0.5	0.5	0.71	0.5	0.3	0.5	0.5	0.5	0.3	0.5	5.0	0.22	0.1	1.7456953993
0.8															1.7056750838
	0.5														1.7245734867
		1.0													1.7158252822
			-0.8												1.7145645911
				7.00											1.7036163753
					1.0										1.7656743812
						0.5									1.7256547510
							- 1.0								1.7285679492
								1.0							1.7849796959
									1.0						1.8056376405
										0.5					1.7799954532
											0.8				1.7605793399
												10.0			1.7202736734
													0.30		1.7196716356
														0.5	1.7257036352

The effect of convective heating, represented by the Biot number (Bi) in Fig. 17, is depicted. The Biot number describes the relative physical importance of surface convection vs internal conduction. A higher Biot number (surface convection) causes a higher surface temperature, which in turn causes a thicker thermal boundary layer. Analysing the influence of the Mass lessening time parameter (ζ) scheduled the temperature distributions seen in Fig. 18. It can be seen from this graph that as the mass relaxation time parameter(γ) is increased, the concentration profiles are reduced. In Figure 19, we see the results of an investigation into in what way the Schmidt number (Sc) affects the concentration map. Schmidt number Sc stands for the ratio of energy to mass diffusivities which has a physical meaning. For this reason, the concentration field weakens with increasing Schmidt number Sc because larger values of mass diffusivity have less effect on the surrounding medium.

Table-3.: Distinct values of Pr, R, γ, Q, Nb, Nt, Du and Bi are given by numerical values of frequency of heat transfer coefficient (Nu).

Pr	*R*	*γ*	*Q*	*Nb*	*Nt*	*Du*	*Bi*	*Nu*
0.71	0.5	0.3	0.5	0.5	0.3	0.5	5.0	0.8657546504
7.00								0.8256475482
	1.0							0.8956095626
		0.5						0.8303343631
			- 1.0					0.8367777475
				0.8				0.8850573629
					0.5			0.8995783437
						1.0		0.9197637363
							10.0	0.8214510842

Table-4.:Different values of Nb, Nt, Sr, Sc and ζ are given by numerical values of the rate of transportation of mass coefficient (Sh).

Nb	*Nt*	*Sr*	*Sc*	*ζ*	*Sh*
0.5	0.3	0.1	0.22	0.1	1.1256427604
0.8					1.0556740963
	0.5				1.1557404796
		0.3			1.1401949345
			0.30		1.0845843322
				0.5	1.1075697837

Table-2 demonstrates the numerical Skinfriction coefficient(Cf) values aimed at changes in the values consisting of the technical parameters like M, K, λ, fw, Pr, R, γ, Q, Sr, Du, Nt, Nb, Bi, Sc and ζ. From this table, it is noticed that the Skin-friction coefficient is growing with mounting values of R, Sr, Du, Nt, Nb, it declines as the values of M, K, λ, fw, Pr, γ, Q, Bi, Sc and ζ augments Table 3 displays the numerical values of the rate of heat transfer coefficient in terms of the Nusselt number (Nu) for various values of Pr, R, γ, Q, Nb, Nt, Du, and Bi. Heat transfer coefficient rate steadily augments with mounting values of R, Nb, Nt, and Du, but the opposite impact is seen with increasing values of Pr, γ, Q, and Bi.Table-4 discusses the impact of Nb, Nt, Sr, Sc, and ζ mass transfer coefficient rate, or with regard to the coefficient of Sherwood number (Sh). From this table, it can be seen that the reduced transportation of mass coefficient rate rises through increasing Nt and Sr values while falling with rising Nb, Sc, and ζ.

Conclusions:

This research establishes the steady, two-dimensional, viscous, incompressible, electrical conduction Maxwell fluid with nanofluid towards a stretching sheet by considering Cattaneo-Christov diffusion, thermal diffusion (Soret), diffusion thermo (Dufour), a porous medium, thermal radiation, a magnetic field, and convective boundary conditions. Similarity transformations is convert the present fluid basic equations obsessed by ordinary differential equations. The Skin-friction coefficient, Nusselt number, and Sherwood numbers are tabulated, and visuals shows how engineering factors affect flow fields, including velocity, temperature, and concentration profiles. Conclusion:

- The thinner the boundary layer, the lower the velocities and the greater the Deborah number, which shows elastic properties that impede flow.
- Rising thermal radiation has accelerated temperature profiles.
- The Soret number increases thermal distribution, whereas the Dufour number increases both.
- The Cattaneo-Christov model has a lower temperature than the Fourier law.
- Fick's concentration is higher than Cattaneo- Christov's.
- The finite element and numerical methods accord well.

References

1. J. Harris, Rheology and Non-newtonian Flow, Longman, New York (1977).
2. J. C. Maxwell, On the dynamical theory of gases, the Kinetic Theory of Gases: An Anthology of Classic Papers with Historical Commentary, (2003), pp. 197-261.
3. X. H. Zhang, R. Shah, S. Saleem, N. A. Shah, Z. A. Khan, J. D. Chung, Natural convection flow Maxwell fluids with generalized thermal transport and Newtonian heating, Case Stud. Therm. Eng., 27 (2021), Article 101226.
4. K. Sadeghy, A. H. Najafi, M. Saffaripour, Sakiadis flow of an upper-convected Maxwell fluid, Int. J. Non Lin. Mech., 40 (2005), pp. 1220-1228.
5. T. Hayat, Z. Abbas, M. Sajid, Series solution for the upper-convected Maxwell fluid over a porous stretching plate, Phys. Lett., 358 (2006), pp. 396-403.
6. H. Li, Y. Jian, Dispersion for periodic electroosmotic flow of Maxwell fluid through a microtube, Int. J. Heat Mass Trans., 115 (2017), pp. 703-713.
7. B. Raftari, A. Yildirim, The application of homotopy perturbation method for MHD flows of UCM fluids above porous stretching sheets, Comput. Math. Appl., 59 (2010), pp. 3328-3337.
8. Vijendra Singh, Agarwal Shweta, MHD flow and heat transfer for Maxwell fluid over an exponentially stretching sheet with variable thermal conductivity in porous medium, Therm. Sci., 18 (2014), pp. 599-615.
9. Muhammad Naveed Khan, Naeem Ullah, Sohail Nadeem, Transient flow of Maxwell nanofluid over a shrinking surface: numerical solutions and stability analysis, Surface. Interfac., 22 (2021), Article 100829, 10.1016/j.surfin.2020.100829

10. M. N. Khan, S. Nadeem, MHD stagnation point flow of a Maxwell nanofluid over a shrinking sheet (multiple solutions), Heat Tansfer, 50 (2021), pp. 4729-4743.
11. Billal M., Sagheer M., Hussain S., Three dimensional MHD upper-convected Maxwell nanofluid flow with nonlinear radiative heat flux, Alex Eng J, 57 (3) (2018), pp. 1917-1925.
12. Singh N. K., Premachandran B., A coupled level set and volume of fluid method on unstructured grids for the direct numerical simulations of two-phase flows including phase change, Int J Heat Mass Transfer, 122 (2018), pp. 182-192.
13. Sheikholeslami M., Darzi M., Sadoughi M. K., Heat transfer improvement and pressure drop during condensation of refrigerant-based nanofluid; an experimental procedure, Int. J. Heat Mass Transfer, 2 (2018), pp. 643-650.
14. J. B. J. Fourier, Théorieanalytique de la chaleur, Académie des Sciences, Paris (1822), p. 3.
15. C. Cattaneo, Sulla conduzione del calore, Atti Semin Mat FisUniv Modena Reggio Emilia, 3 (1948), pp. 83-101.
16. C. I. Christov, On frame indifferent formulation of the Maxwell-Cattaneo model of finite-speed heat conduction, Mech. Res. Commun., 36 (4) (2009), pp. 481-486.
17. M. G. Reddy, M. V. V. N. Rani, K. G. Kumar, B. C. Prasannakumar, A. J. Chamkha, Cattaneo-Christov heat flux model on Blasius-Rayleigh-Stokes flow through a transitive magnetic field and Joule heating, Physica, 548 (2020), Article 123991.
18. M. Haneef, M. Nawaz, S. O. Alharbi, Y. Elmasry, Cattaneo-Christov heat flux theory and thermal enhancement in hybrid nano Oldroyd-B rheological fluid in the presence of mass transfer, Int. Commun. Heat Mass Tran., 126 (2021), Article 105344.
19. R. J. P. Gowda, F. S. A. Mubaddel, R. N. Kumar, B. C. Prasannakumara, A. Issakhov, M. R. Gorji, Y. A. A. Turki, Computational modelling of nanofluid flow over a curved stretching sheet using Koo-Kleinstreuer and Li (KKL) correlation and modified Fourier heat flux model, Chaos, Solit. Fractals, 145 (2021), Article 110774.
20. F. S. A. Mubaddel, U. Farooq, K. A. Khaled, S. Hussain, S. U. Khan, M. O. Aijaz, M. R. Gorji, H. Waqas, Double stratified analysis for bioconvection radiative flow of Sisko nanofluid with generalized heat/mass fluxes, Phys. Scripta, 96 (2021), Article 055004.
21. Ijaz M., Ayub M., Nonlinear convective stratified flow of Maxwell nanofluid with activation energy, Heliyon, 5 (1) (2019), Article e01121.
22. S. A. Shehzad, T. Hayat, A. Alsaedi, M. A. Meraj, Cattaneo-Christov heat and mass flux model for 3D hydrodynamic flow of chemically reactive Maxwell liquid, Appl. Math. Mech., 38 (2017), pp. 1347-1356.
23. T. Hayat, M. I. Khan, M. Farooq, T. Yasmeen, A. Alsaedi, Stagnation point flow with Cattaneo-Christov heat flux and homogeneous-heterogeneous reactions, J. Mol. Liq., 220 (2016), pp. 49-55.
24. M. Mustafa, Cattaneo-Christov heat flux model for rotating flow and heat transfer of upper-convected Maxwell fluid, AIP Adv., 5 (4) (2015), Article 047109.
25. F. Abbasi, M. Mustafa, S. Shehzad, M. Alhuthali, T. Hayat, Analytical study of Cattaneo-Christov heat flux model for a boundary layer flow of Oldroyd-B fluid, Chin. Phys. B, 25 (1) (2015), Article 014701.

26. M. Waqas, T. Hayat, M. Farooq, S. Shehzad, A. Alsaedi, Cattaneo-Christov heat flux model for flow of variable thermal conductivity generalized Burgers fluid, J. Mol. Liq., 220 (2016), pp. 642-648.
27. S. Shehzad, F. Abbasi, T. Hayat, B. Ahmad, Cattaneo-Christov heat flux model for third-grade fluid flow towards exponentially stretching sheet, Appl. Math. Mech., 37 (6) (2016), pp. 761-768.
28. S. Han, L. Zheng, C. Li, X. Zhang, Coupled flow and heat transfer in viscoelastic fluid with Cattaneo-Christov heat flux model, Appl. Math. Lett., 38 (2014), pp. 87-93.
29. B. A. S. A. Liaqat Ali, Xiaomin Liu, R. M. Zulqarnain, Finite element analysis of unsteady MHD Blasius and Sakiadis flow with radiation and thermal convection using Cattaneo-Christov heat flux model, Phys. Scr., 71 (2021), Article 095010.
30. S. Mukhopadhyay, Heat transfer analysis of the unsteady flow of a Maxwell fluid over a stretching surface in the presence of a heat source/sink, Chinese Physics Letters, vol. 29, Article ID 054703, 2012.
31. K. Sadeghy, H. Hajibeygi, and S. M. Taghavi, Stagnation point flow of upper-convected Maxwell fluids, International Journal of Non-linear Mechanics, vol. 41, no. 10, pp. 1242-1247, 2006.